*Environ Res Tec, Vol. 7, Issue. 3, pp. 422–434, September 2024*

**Environmental Research and Technology**
https://ert.yildiz.edu.tr - https://dergipark.org.tr/tr/pub/ert
DOI: https://10.35208/ert.1446909

Environmental Research & Technology

**Research Article**

# Crop cover identification based on different vegetation indices by using machine learning algorithms

**Saurabh PARGAIEN[1], Rishi PRAKASH[*,1], Ved Prakash DUBEY[2], Devendra SINGH[2]**

*[1]Department of Electronics and Communication Engineering, Graphic Era (Deemed to be University), Dehradun, Uttarakhand, India*
*[2]Department of Computer Sciences and Engineering, Graphic Era Hill University, Dehradun, Uttarakhand, India*

## ARTICLE INFO

*Article history*
Received: 05 March 2024
Revised: 04 April 2024
Accepted: 20 April 2024

**Key words:**
ARIMA; BNDVI; GNDVI; LSTM; MSE; NDVI

## ABSTRACT

In this article, three different indices NDVI, BNDVI and GNDVI are used for the identification of wheat, mustard and sugarcane crop of Saharanpur district's region of Uttar Pradesh. Sentinel 2B satellite images are collected from October 02, 2018 to April 15, 2019. These images are processed using Google Earth Engine. These sentinel images are used to generate NDVI, BNDVI and GNDVI images using GEE. These three different indices images are further processed using SNAP software and particular indices values for 210 different locations are calculated. The same process is used for calculating BNDVI and GNDVI values. ARIMA, LSTM and Prophet models are used to train the time series indices values (NDVI, BNDVI and GNDVI) of wheat, mustard and sugarcane crop. these models are used to analyse MSE (mean absolute percentage error) and RMSE values by considering various parameters. Using ARIMA Model, for wheat crop GNDVI indices shows minimum RMSE 0.020, For Sugarcane crop NDVI indices shows minimum RMSE 0.053, For Mustard crop GNDVI indices shows minimum RMSE 0.024. Using LSTM model, for wheat crop NDVI indices shows minimum RMSE 0.036, For Sugarcane crop BNDVI indices shows minimum RMSE 0.054, For Mustard crop GNDVI indices shows minimum RMSE 0.026. Using Prophet model, for wheat crop GNDVI indices shows minimum RMSE 0.055, For Sugarcane crop NDVI indices shows minimum RMSE 0.088, For Mustard crop GNDVI indices using Prophet model shows minimum RMSE 0.101.

**Cite this article as:** Pargaien S, Prakash R, Dubey VP, Singh D. Crop cover identification based on different vegetation indices by using machine learning algorithms. Environ Res Tec 2024;7(3)422–434.

## INTRODUCTION

The frequent availability of satellite images opens up a multitude of opportunities for scientists engaged in phenological investigation and crop classification. Understanding various land use classes, such as built-up areas, rivers, bare soil, forests, and farmland, requires the selection of an appropriate technique [1]. Satellite images can be used to forecast Earth's surface analyses at various sizes and resolutions. Satellite images can be used to access and analyse all the necessary spectral and spatial feature data for the various land surfaces on Earth [2, 3]. The use of machine learning along with remote sensing images makes it more acceptable for the land use land cover classification. Multi-temporal images are used to extract crop features based on time [4]. Using spectral curves, the earthly objects are categorised. The radiant energy emitted by the items in the ground is the foundation of these spectral curves. Numerous indices are employed to categorise data to differentiate crops on the basis of dif-

***Corresponding author.**
*E-mail address: rishi.prakas@gmail.com

ferent characteristics [5]. Data mining and ML techniques have been used in many real-world applications. Traditional ML techniques make the assumption that training and testing statistics came from the same domain and have a similar input feature space and set of data distribution properties [6]. In other situations, collecting training data is impractically expensive, time-consuming, and difficult in rural areas [7]. Therefore, it is necessary to develop high-performance learners using information that may be more easily obtained from many sources. Many CNN based techniques (such ResNet, VGG, and Inception) have been built in the domains of artificial intelligence, language processing, medical domain, and remote sensing application [8, 9]. Deep learning helps in target identification and classification. DL methods typically depend on enormous volumes of tagged training data. Big, potent deep learning models have been known for being data-hungry. They must be trained with thousands of data points before they can produce an accurate forecast. Resources and time are both quite expensive when it comes to training [10]. Whereas, ML algorithms typically operate independently. Over a huge dataset, it gains knowledge about how to perform a certain task. It is impossible to use previous knowledge when analysing a new task. For the algorithm to start learning again, it usually needs a second dataset. To improve performance, a pre-trained CNN can be tuned on a particular dataset. Moreover, it reduced the target labelled data in comparison to starting from scratch [11, 12].

Transfer learning is the process of using previously learned tasks to learn new ones. The necessary data can be recorded and accessed by the algorithm. The model is loaded with features. Transfer learning is a ML technique that builds a model for one job on top of a model generated for another task. This transfer learning strategy has two major benefits: First and foremost, transfer learning accelerates learning. Since the algorithm does not have to learn as many new things, it can generate high-quality results more rapidly. Transfer learning, on the other hand, requires less data. In conventional learning, a sufficient amount of training data-which may number in the millions-must be fed to an algorithm before it can learn new knowledge. It is possible that the cost to generate and prepare this data for the model will be too high or that it won't be available at all. The issue of inadequate training information for the target task is frequently addressed through the use of transfer learning [13, 14]. The BA-based clustering technique has been suggested as a solution to crop type classification issues using multispectral satellite images [15]. This study created a new plant feature band set (FBS), optimised it, and combined it with an object-oriented classification (OOC) technique to create a new crop classification method. To distinguish different types of vegetation, 20 spectral indices sensitive to the biological factors of the vegetation are added to the FBS in addition to the spectral and textural aspects of the original image. Additionally, a class-pair separability (CPS) based spectral dimension optimization approach of FBS is suggested to enhance class pair separability while minimising data redundancy [16]. Several spectral indices have been generated using the time sequences of Landsat ETM+ and Rapid Eye data, and a framework for classification based on HMMs was developed for modelling crop vegetation patterns over a rural Mediterranean area with significant spatiotemporal crop variability [17]. A total of 12 commonly used spectral vegetation indicators were computed using 14 Sentinel-2 images. Principal component analysis (PCA) was also employed to evaluate the impact of decreased dimensionality on crop type mapping accuracy. The four original PCA components were processed in order to examine classifications for each index alone as well as for groups of various indices, all under the supervision of RF [18]. This article examined the use of optical imagery data in a multi-temporal crop type identification based on very high-resolution spatial imaging. Utilizing the red, green, and near-infrared spectral bands, three vegetation indices (VIs), including the NDVI, GNDVI and SAVI were created using the images of WorldView-3 and Sentinel-2 between April and July 2016 over Coalville (UK). The combination of DT and RF classification algorithms was predicted to have an OA of 91% [19]. The significance of 82 calculated indices for categorising crop types was assessed. Cropland categorization using MSI data was carried out using RF and SVM. Overall accuracy of 90.2–92.2% was achieved using Super learning [20]. The MSI data were used to produce 91 spectral indices [21]. A method for compositing the multi-temporal NDVI to map the locations for planting winter crops using optical data from Landsat-7, -8, and Sentinel-2 was suggested in this article [22]. For crop mapping, the RF classifier-PSO ensemble method was employed [23]. SVM, RF and XG Boost using known vegetative indicators (VIs) were also used [24]. SDA and RF, two feature selection and evaluation techniques, were used to determine the red edge vegetation index of the NDRE based on PCA [25]. The three most important reflectance bands for crop classification, in our opinion, are SWIR1, Green, and Red Edge2. The LSWI, NDWI, and EVI were the top three vegetation indicators for crop classification [26]. SVM, RF, CNN, RNN with LSTM, and RNN with GRU models were analysed to perform crop classification [27]. Phenological cycles of crops are explored utilising temporal NDVI patterns. By compiling spectral data from various phenological stages, most crops with comparable spectral properties may be recognised [28]. Land surface temperature (LST) and the NDVI was used to improve crop categorization accuracy [29]. The Double Exponential Smoothing and Autoregressive Integrated Moving Average with Explanatory Variables ensemble was created to improve prediction performance using forecasting models based on time series analysis [30]. Using four different approaches—KELM, multilayer feedforward NNs, RF, and SVM—six crop kinds— beetroot, beans, winter wheat, grass, potato and maize were recognized from one MSI image and five C-SAR images collected during the year 2016 [31]. Landsat 8 OLI multi-temporal data of year 2013 was employed to find 7 crops varieties in Northern Italy. The study investigated the relationship between crop map delivery time and accuracy using four supervised algorithms that were fed multi-temporal spectral indices (EVI, NDFI, and RGRI) during the course of the season [32, 33]. Nineteen

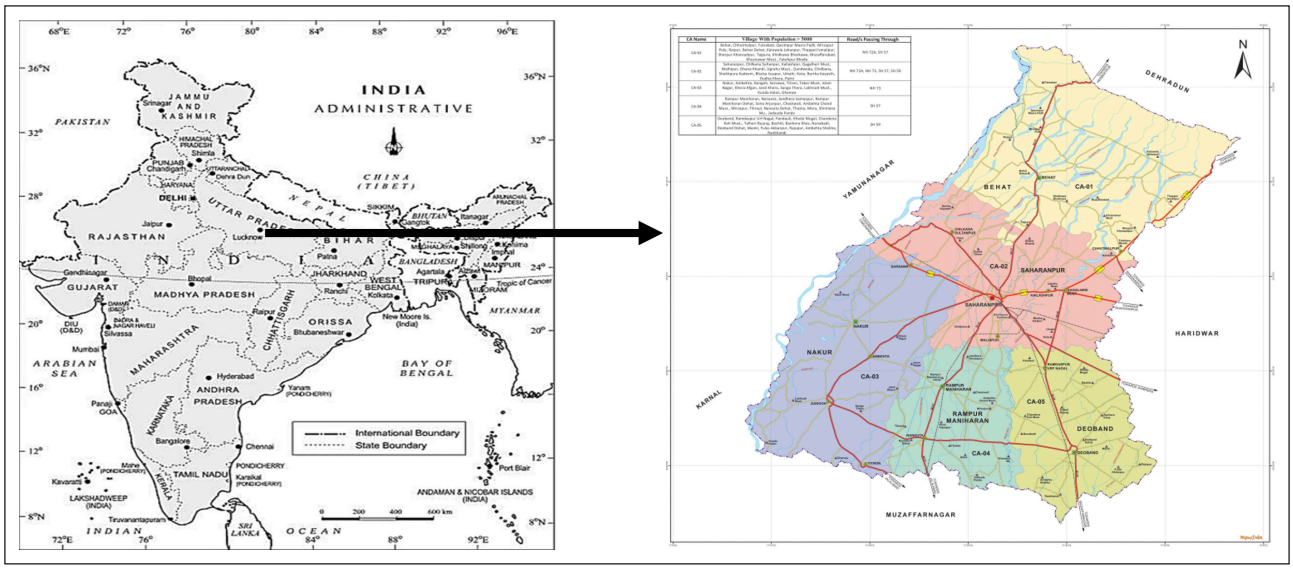


**Figure 1**. Saharanpur District map, Uttar Pradesh, India.

multitemporal images captured by the Landsat-8 and Sentinel-1A RS satellites are used in experiments for the joint experiment of agricultural assessment and monitoring test site in Ukraine to classify crops in a heterogeneous environment using ML methods [34]. A supervised classification is carried out using a group of MLP classifiers for broad area crop mapping at the JECAM test site in Ukraine. The MLP committee achieves an overall classification accuracy of 85% (OA=85.32% and Kappa 0.8235). Accuracy for Winter wheat, winter rapeseed, maize, and sugar beet were 85%. Sunflower, soybeans, and spring crops show poor performance [35]. This study compares two methods for classifying crops using multitemporal optical (Landsat-8) and synthetic-aperture radar (SAR) Sentinel-1 imagery: pixel-based and parcel-based methods for the Joint Experiment of Crop Assessment and Monitoring test site in Ukraine, which will encompass the Odessa and Kyiv oblasts in 2014 and 2015, respectively [36]. According to this study, phenology-based algorithms can be recognised for classifying crops across a wide area. Annual maps of winter crops with UA 96.61%, PA 94.13%, OA 94.56%, and Kappa coefficient of 0.89 were produced using rule-based algorithms and decision trees [37].

## MATERIALS AND METHODS

### Study Area and Data Set Used

The study area lies in Saharanpur district of Uttar Pradesh in India which is located 29° 57' 34.8984" N latitudes and 77° 32' 56.6052" E as shown in Figure 1. Saharanpur district is located in the north part of the India near the foothills of Shivalik ranges and lies in the Doab region. The area of Saharanpur district is 3689 sq. km. It is one of the most agriculturally developed districts of Uttar Pradesh. The important crops of the region are wheat, rice, maize, jawar, bajara, sugarcane and mustard. Wheat, sugarcane, and mustard were chosen for this study because they are the main crops grown in the study area during the winter. The climate in Saharanpur district is warm where the temperate ranges from 5 °C to 45 °C with an annual average temperature of 23 °C. The range of humidity of Saharanpur region varies from 34% to 84%. In winter season its ranges from 62% to 74%, in summer season its ranges from 34% to 54% and in rainy season its ranges from 80% to 84%. The annual rainfall ranges from 498 to 1566 mm with an average rainfall value of 1027 mm. The district's soil composition consists primarily of coarse sandy loam, with some pockets of clay loam. There is a 6.8 to 8.2 PH range. In general, the subsurface water quality is good.

This study utilizes Sentinel – 2B level 1 C data. Level-1C product provides orthorectified Top-of-Atmosphere (TOA) reflectance, with sub-pixel multispectral registration. The Level-2A processing includes a Scene Classification and an Atmospheric Correction applied to Top-of-Atmosphere (TOA). With a revisit time of two to three days at mid-latitudes and five days at the equator, Sentinel-2B offers a high level of temporal resolution, increasing the likelihood of finding images free of clouds or scenes that have less cloud cover. Sentinel-2's high spatial resolution (10, 20, and 60 m pixels for different spectral bands) makes it possible to identify and eliminate clouds and cloud shadows with greater accuracy. With 13 bands spanning from the visible to the shortwave infrared, the broad spectral range makes it possible to distinguish between clouds and surface characteristics using a variety of indices and algorithms. This study identifies wheat, sugarcane and mustard crops of Saharanpur region using NDVI, BNDVI and GNDVI indices. Sentinel – 2B data between October 2018 to April 2019 was observed for this study whose details are provide in Table 1.

This paper focuses on the identification of different crops using three ML models. A flow chart of modelling approach is shown in Figure 2. Wheat, sugarcane and mustard crop has been used to identify from the study area by utilizing ARIMA, LSTM and Prophet models. RMSE and MSE values were computed for all models to determine the most suitable ML model and vegetation indices to identify the

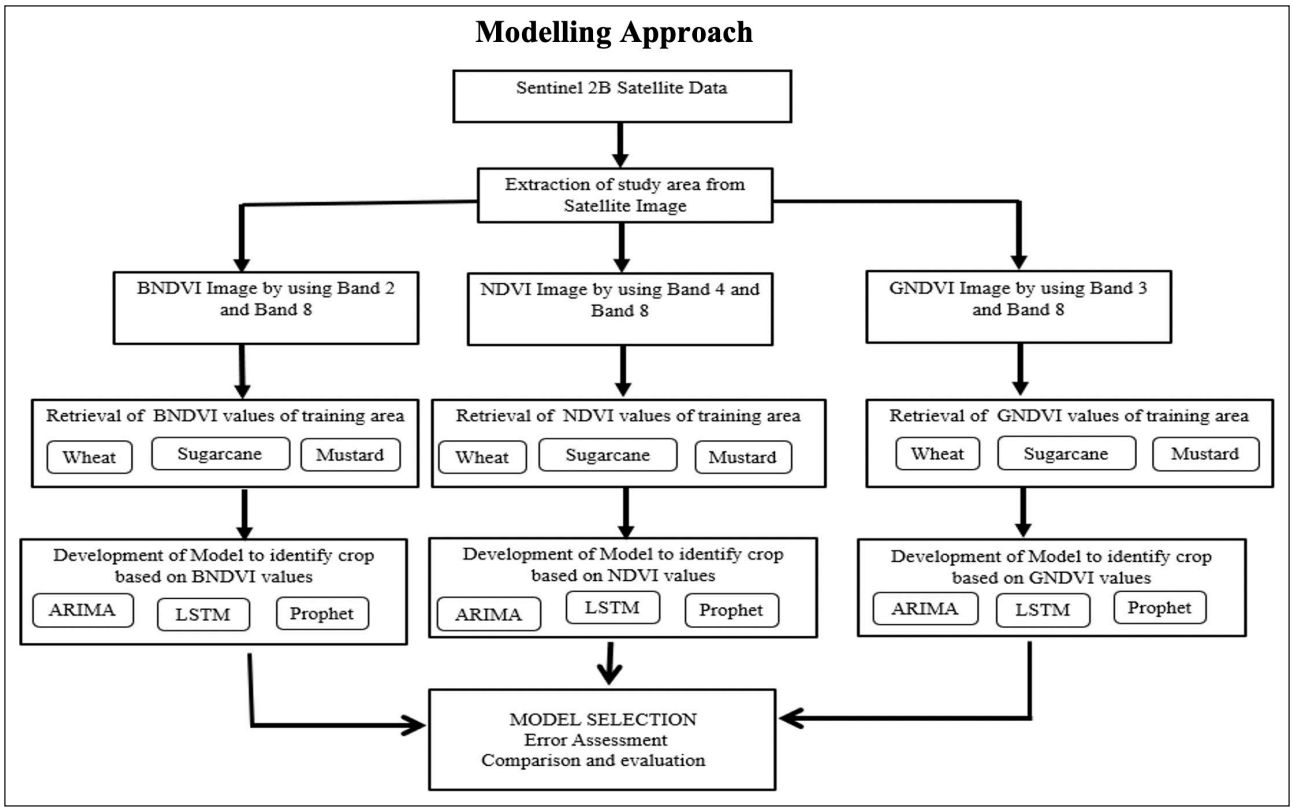


**Figure 2**. The methodology used for crop identification.

specific crop. Following steps were performed to identify different crops based on ML approach:

Step 1: Sentinel – 2B satellite images of study area was processed using GEE. As a first step, the images of study area were extracted and vegetation indices images were formed with the help of GEE. NDVI, BNDVI and GNDVI images were formed to identify different crop.

Step 2: Machine learning models require training data set to train the selected model. Therefore, for each crop, i.e., wheat, sugarcane and mustard the training data set of vegetation indices, i.e., NDVI, BNDVI and GNDVI were extracted with the help of SNAP software. 15 different areas within the study area were selected to determine the indices values. A dataset of 210 points was created for three different crops using three different vegetation indices.

Step 3: Univariate time series models based on ARIMA, LSTM and Prophet were developed with vegetation indices, i.e., NDVI, BNDVI and GNDVI for each crop, i.e., wheat, sugarcane and mustard. These developed models were further used to predict the different crop based on vegetation indices.

Step 4: RMSE and MSE were evaluated for different models for the prediction of crop based on the vegetation indices. A comparison of ML models and vegetation indices were carried out to access the suitability of predication of specific crop.

Total 210 ground points of wheat, mustard and sugarcane were collected during this duration of the study area. 180 sample points are used to train the ARIMA, LSTM and Prophet model and 30 sample points are used for validation.

**Table 1.** Details of Sentinel 2B data used in the study

| S. No. | Acquisition date | Sensor | Spatial resolution | Cloud cover |
|---|---|---|---|---|
| 1 | 02-Oct-18 | | | |
| 2 | 18-Oct-18 | | | |
| 3 | 05-Nov-18 | | | |
| 4 | 21-Nov-18 | | | |
| 5 | 08-Dec-18 | | | |
| 6 | 21-Dec-18 | | | |
| 7 | 15-Jan-19 | Sentinel | 10 | Less than |
| 8 | 28-Jan-19 | 2B | meters | 10% |
| 9 | 09-Feb-19 | | | |
| 10 | 26-Feb-19 | | | |
| 11 | 06-Mar-19 | | | |
| 12 | 26-Mar-19 | | | |
| 13 | 02-Apr-19 | | | |
| 14 | 15-Apr-19 | | | |

**Machine Learning Models to Train the Vegetation Indices**

Three ML models ARIMA, LSTM and Prophet has been utilised in this study. Following paragraphs provide a brief description of these ML models.

***a) ARIMA Model***

The ARIMA model, also known as the Autoregressive Integrated Moving Average Model, is a prominent stochastic time series model that was established in the literature. The time series is shown to be regressed on its own historical data by the AR component of ARIMA. The prediction error is a linear combination of the corresponding previous errors, according to the MA component of ARIMA. As required by the ARIMA model technique, the I part of ARIMA illustrates how the data values have been substituted with differenced values of d in order to obtain data that is stationary. The time series under consideration is linear and has a normal distribution, which is the essential premise upon which this model is built. This model is employed in time-series analysis. It entails looking for patterns in the data and then forecast events based on those patterns. To capture various facets of a time series, the model integrates three elements: moving averages, differencing, and autoregression. In order to create an ARIMA model, the proper parameters must be chosen using strategies like grid search and cross-validation. An ARIMA model has three order parameters: p, d, and q. The number of lag observations, or lag order, in the model is represented by the symbol p. The symbol d denotes the degree of differencing, which is used to represent the number of differences between raw observations. The moving average window's size, or the moving average's order, is represented by the symbol q. $\beta_i$ is the auto regressive parameter of order p, $\emptyset_i$ is moving average parameter of order q, α and μ are constant, $y_t'$ prediction estimate at time t, ϵ error term, t is integer index. Auto ARIMA (p, d, and q) automatically generates the most suitable parameter values. The best values that were created will be used by the model to produce accurate forecast results. Only past values (lags) are used by the AR model to predict future values. The AR model in its generalized form is expressed in equation 1.

$$AR(p): x_t = \alpha + \sum_{i=1}^{p} \beta_i x_{t-i} + \epsilon \quad (1)$$

The amount of prior values "p" will be considered for deciding the forecast value. More historical values will be considered as the model's order increases. To difference the data, the difference between consecutive observations is computed. Mathematically, it can be shown in equation 2.

$$y_t' = y_t - y_{t-1} \quad (2)$$

Differencing removes the changes in the level of a time series, eliminating trend and seasonality and consequently stabilizing the mean of the time series. On the other hand, the moving-average, MA, model relies on previous forecasting failures to produce predictions. The MA model in its generalized form is expressed in equation 3.

$$MA(q): x_t = \mu + \sum_{i=1}^{q} \emptyset_i \epsilon_{t-1} \quad (3)$$

The linear combination of q historical forecast errors can be thought of as the MA model. For predicting time series, ARIMA models have a number of benefits, such as the ability to capture a variety of patterns and behaviours in the data, such as seasonality, cycles, or trends. As they only need three parameters and some fundamental statistical assumptions, they are also fairly simple and easy to implement. For the forecasts, these models can include confidence ranges and error metrics like standard errors or root mean squared errors. When predicting time series, ARIMA models can be constrained and difficult. Due to the fact that they are linear models, they are unable to manage complicated dynamics or nonlinear relationships, such as rapid shocks or regime transitions. Before using ARIMA models, the data may need to be pre-processed to remove outliers and missing values, which can have an impact on the model estimation and forecasting performance. They are not appropriate for extremely brief or extremely long time series because they might not have enough data or get unstable with time.

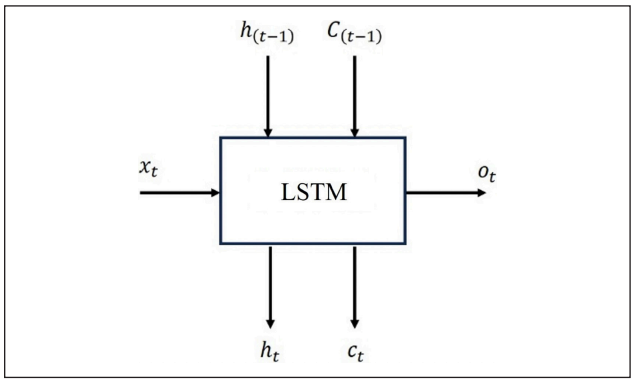


**Figure 3**. LSTM Model.

***b) LSTM Model***

Exploding/vanishing gradient issues are common while learning long-term interdependence. Strong recurrent neural networks like the LSTM model were created expressly to address these issues, even in cases where the minimal time lags are quite large. The LSTM architecture is composed of a group of sub-networks that are linked recurrently. The memory block's functions include data flow control with non-linear gating units and state maintenance over time. Three gates and a cell state give an LSTM module the capacity to learn, unlearn, or retain information from each of the units in a selected manner. In LSTM, the cell state facilitates continuous information transfer between units by permitting a limited number of linear interactions.

$$f_{(t)} = \sigma_g\ (W_f \times x_t + U_f \times h_{t-1} + b_f \quad (4)$$

$$i_{(t)} = \sigma_g\ (W_i \times x_t + U_i \times h_{t-1} + b_i \quad (5)$$

$$o_{(t)} = \sigma_g\ (W_o \times x_t + U_o \times h_{t-1} + b_o \quad (6)$$

$$c'_{(t)} = \sigma_c\ (W_c \times x_t + U_c \times h_{t-1} + b_c \quad (7)$$

$$c_{(t)} = f_{(t)} * c_{(t-1)} + i_{(t)} * c'_{(t)} \quad (8)$$

$$h_{(t)} = o_{(t)} * \sigma_c\ (c_t) \quad (9)$$

The Figure 3 shows the input and outputs of an LSTM for a single time step. This is one time step input; output and the equations are used for a time unrolled representation. Equation 4 represents $f_{(t)}$ (forget gate), equation 5 represents $i_{(t)}$ (input gate), equation 6 represents $o_{(t)}$ (output gate),

equation 7 and 8 represents $c'_{(t)}$ and $c_{(t)}$ (cell gate) respectively, equation 9 represents $h_{(t)}$ (hidden gate), $\sigma_g$ is sigmoid, $\sigma_c$ is tanh and * is element wise multiplication. The input sequence directly or the output of a CNN can be used as the input for the LSTM x(t). These are the inputs from the previous timestep LSTM: $h_{(t-1)}$ and $c_{(t-1)}$. The LSTM's output for this timestep is $o_{(t)}$. In addition, the LSTM produces the $c_{(t)}$ and $h_{(t)}$ that can be utilised by the subsequent time step LSTM. Observe that $f_{(t)}$, $i_{(t)}$, $c'_{(t)}$ are also produced by the LSTM equations. These are utilised to generate $c_{(t)}$ and $h_{(t)}$ for the LSTM's internal consumption. There is no time dependence in the weight matrices $W_f$, $W_i$, $W_o$, $W_c$, $U_f$, $U_i$, $U_o$, $U_c$ and biases $b_f$, $b_i$, $b_o$, $b_c$. This indicates that these weight matrices remain constant throughout time steps.

The LSTM network is used in a variety of problem domains, both alone and in combination with other deep learning designs. LSTM is capable of addressing any problem requiring periodic memory, such as time series forecasts. They are more complicated and require more training data in order to learn efficiently than regular RNNs. Secondly, they are unsuitable for online learning assignments like forecasting or classification tasks where the provided data is not a sequence.

***c) Prophet Model***

Prophet is a time series prediction technique that fits the appropriate seasonality to the non-linear trends in the series using an additive model. It works well with highly seasonal time series and numerous seasons of previous information. The Prophet models' primary inputs are growth and changepoint range. For growth, the trend's "linear" or "logistic" forms are used. In changepoint range, how close the changepoints can be to the time series' end depends on the range. The trend is more malleable as the value increases. It consists of two seasonal components: a weekly-based model using dummy variables, and an annual-based model using Fourier series. In Prophet model, there is no need of much prior experience in forecasting time series data. With a set of data, it is capable of recognizing seasonal patterns and offers easily understood characteristics. Prophet has a number of advantages over other models, one of which being its interpretability. For seasonality, there are smoothing parameters that let you control how closely to fit historical cycles. When compared to the forecasting model with no change, Prophet did not offer any overall improvement.

Prophet can be considered a nonlinear regression model, of the form as shown in equation 10.

$$y_t = g(t) + s(t) + h(t) + \epsilon_t \quad (10)$$

where s(t) reflects the different seasonal patterns, h(t) records the effects of the holidays, and εt is a white noise error term. g(t) represents a piecewise-linear trend (or "growth term").

**Accuracy Assessment**

Accuracy assessment is important to determine the strength of model in predicting the unknown. The assessment of accuracy can be performed based on evaluating the error between the actual and prediction. Therefore, in this paper Root mean square error and mean square error are calculated and analysed. RMSE and MSE are explained below

***a) RMSE***

One of the most popular metrics for assessing the accuracy of forecasts is the root mean square error, often known as the root mean square deviation. It uses the Euclidean distance to illustrate the deviation between predicted and measured true values. Mean Squared Error (MSE) and Root Mean Squared Error (RMSE) are regression measures that are actually connected because RMSE's computation is based on MSE.

$$\text{RMSE}=\sqrt{\frac{\sum_{i=1}^{N}\left\|y(i)-\widehat{y(i)}\right\|^2}{N}} \quad (11)$$

RMSE is explained by equation 11, where N is the number of data points, y(i) are the observed values, and y'(i) are the predicted values.

***b) MSE***

The average squared difference between the actual and expected numbers is known as the mean squared error. Squared error is a row-level error calculation that squares the difference between the real and the predicted. It is also frequently referred to as L2 loss. By looking at the MSE, or mean of these errors, we may assess the model's performance more accurately throughout the whole dataset. One of the most used measures when working with regression models is RMSE, which is usually chosen more than MSE. This is mainly because the resulting number has a much easier to understand interpretation due to its substantially bigger value.

$$\text{MSE}=\frac{\sum_{i=1}^{N}\left\|y(i)-\widehat{y(i)}\right\|^2}{N} \quad (12)$$

MSE is explained by equation 12, where y(i) represents the observed values, N is the number of data points, and y'(i) represents the predicted values.

We utilise the RMSE more frequently when evaluating a model's fit to a dataset since its units of measurement match those of the response variable. The MSE, on the other hand, is expressed in response variable squared units.

## RESULT AND DISCUSSION

**Determination of Vegetation Indices and Preparation of Training Data**

The NDVI, GNDVI, and BNDVI images can be calculated using the red, near-infrared, green, and blue bands available in Sentinel satellite images. The GEE Code Editor can be accessed by going to code.earthengine.google.com using GEE. The "COPERNICUS/S2" image collection contains Sentinel 2 data, which needs to be imported. We must first supply the region of interest (ROI) in order to compute the vegetation indices. We can construct a geometry object for our ROI. It is necessary to decide on the analysis's time frame. We need to filter the Sentinel-2 data based on our time range and ROI. The image from each day with the fewest clouds must be se-

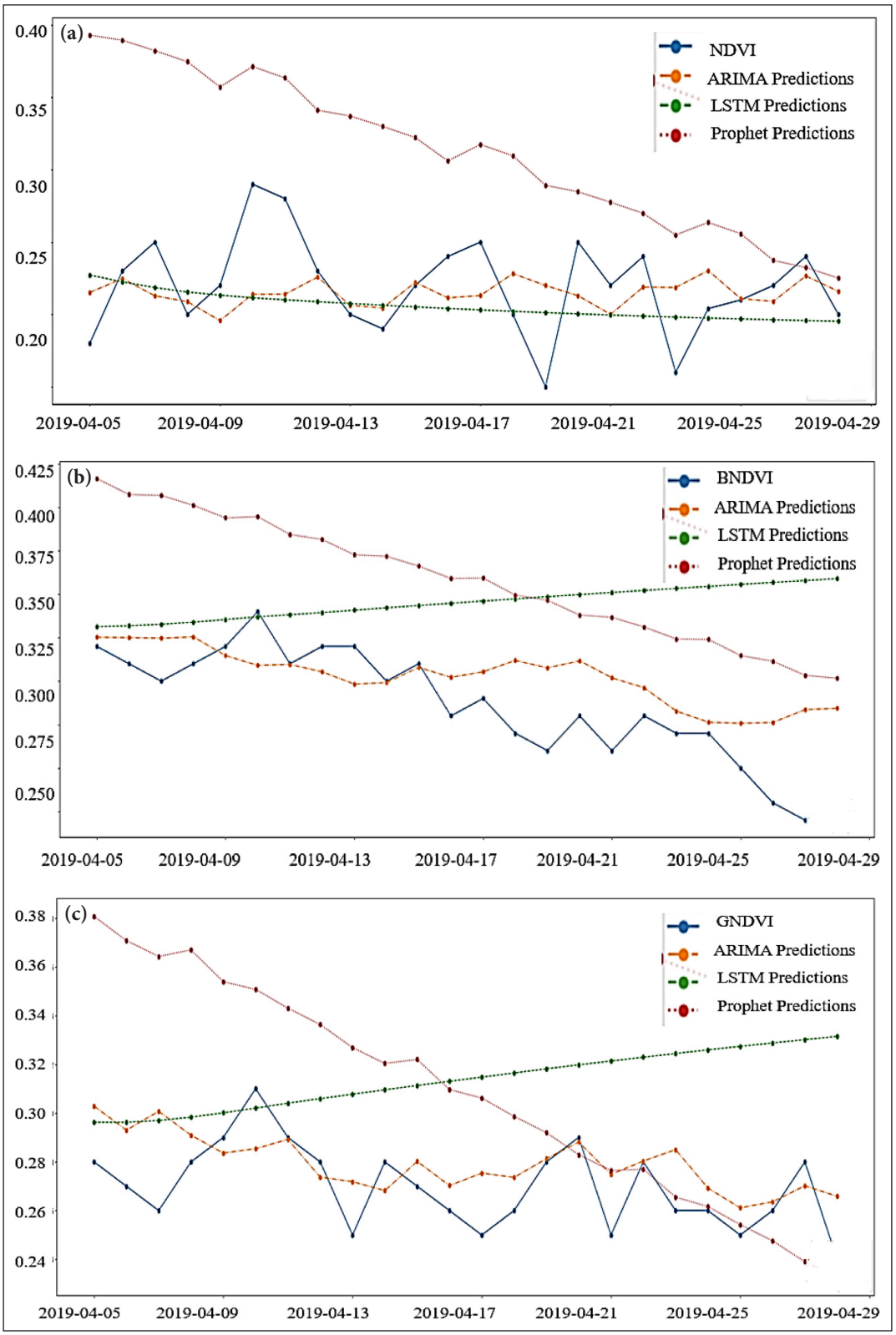


**Figure 4**. **(a)** NDVI indices predicted graph for ARIMA, LSTM and Prophet model. **(b)** BNDVI indices predicted graph for ARIMA, LSTM and Prophet model. **(c)** GNDVI indices predicted graph for ARIMA, LSTM and Prophet model.

lected after the collection has been sorted by cloud cover. We can compute these vegetation indices by creating a function to do so and mapping it across the collection of images. We will then see the NDVI, GNDVI, and BNDVI images on the map. We can adjust the visualisation settings (min, max, and palette) to suit our tastes. Following the processing of the study area's NDVI, BNDVI, and GNDVI images with GEE, the SNAP software is used to further process the images and determine the region of interest's indices values. The specific index values for 210 distinct points are determined.

**Table 2a.** NDVI indices RMSE and MSE Errors for ARIMA, LSTM and Prophet model

| | Wheat NDVI | | |
|---|---|---|---|
| S. No. | Models | RMSE errors | MSE errors |
| 0 | ARIMA | 0.0345 | 0.0012 |
| 1 | LSTM | 0.0367 | 0.0013 |
| 2 | Prophet | 0.1072 | 0.0115 |

**Table 2b.** BNDVI indices RMSE and MSE Errors for ARIMA, LSTM and Prophet model

| | Wheat BNDVI | | |
|---|---|---|---|
| S. No. | Models | RMSE errors | MSE errors |
| 0 | ARIMA | 0.0300 | 0.0009 |
| 1 | LSTM | 0.0548 | 0.0030 |
| 2 | Prophet | 0.0748 | 0.0056 |

**Table 2c.** GNDVI indices RMSE and MSE Errors for ARIMA, LSTM and Prophet model

| | Wheat GNDVI | | |
|---|---|---|---|
| S. No. | Models | RMSE errors | MSE errors |
| 0 | ARIMA | 0.0200 | 0.0004 |
| 1 | LSTM | 0.0509 | 0.0026 |
| 2 | Prophet | 0.0556 | 0.0031 |

**Table 3a.** NDVI indices RMSE and MSE Errors for ARIMA, LSTM and Prophet model

| | Sugarcane NDVI | | |
|---|---|---|---|
| S. No. | Models | RMSE errors | MSE errors |
| 0 | ARIMA | 0.0538 | 0.0029 |
| 1 | LSTM | 0.0806 | 0.0065 |
| 2 | Prophet | 0.0883 | 0.0078 |

**Table 3b.** BNDVI indices RMSE and MSE Errors for ARIMA, LSTM and Prophet model

| | Sugarcane BNDVI | | |
|---|---|---|---|
| S. No. | Models | RMSE errors | MSE errors |
| 0 | ARIMA | 0.0616 | 0.0038 |
| 1 | LSTM | 0.0547 | 0.0030 |
| 2 | Prophet | 0.0889 | 0.0079 |

**Table 3c.** GNDVI indices RMSE and MSE Errors for ARIMA, LSTM and Prophet model

| | Sugarcane GNDVI | | |
|---|---|---|---|
| S. No. | Models | RMSE errors | MSE errors |
| 0 | ARIMA | 0.0670 | 0.0045 |
| 1 | LSTM | 0.0741 | 0.0055 |
| 2 | Prophet | 0.0883 | 0.0078 |

**Development of Machine Learning Models**

The ARIMA (Auto Regressive Integrated Moving Average) model is a time series forecasting method that combines autoregressive (AR) and moving average (MA) components. It was developed to capture and model different aspects of time series data, making it a versatile tool for analyzing and predicting time-dependent phenomena. For ARIMA model, the start value of p, d, and q is considered as 0. The maximum value of p and q is 5 and maximum value of d is considered as 8. The maximum value of P, D and Q is considered as 5. The starting value of P, Q is 0 and D is considered as 1. The value of m is 12 and random state is 20. The value of n fits is 5. The Boolean value of seasonal and trace is true. The best ARIMA model of order = (4,0,1), and seasonal order = (2,1,1,12) is considered in this time series analysis.

The LSTM model using "relu" activation functions and a single LSTM layer with 200 neurons. Since there is just one time-step and one feature in this data, the input shape is (1,1). Adam optimization method is used in this analysis. loss function, which can be used to calculate the model's loss and adjust the weights in order to lower the loss on the subsequent evaluation. The loss function in this case is mean square error. The model is trained for 1000 epochs.

The parameter with the greatest impact on the Prophet model is the changepoint prior scale parameter. It establishes the trend's degree of flexibility, namely how much the trend fluctuates at trend changepoints. In this analysis the value of this parameter is 0.5. The seasonality mode parameter is multiplicative.

**Selection of ML Model and Vegetation Indices For Prediction of Crop**

***Wheat Crop***

Figure 4a, 4b and 4c showed NDVI BNDVI, and GNDVI indices predicted graph for ARIMA, LSTM, and Prophet model for wheat crop. Table 2a show RMSE error and MSE error for ARIMA, LSTM, and Prophet model using wheat NDVI indices values. NDVI indices for wheat crop show RMSE errors of 0.0345, 0.0367 and 0.1072 for ARIMA, LSTM, and Prophet model respectively. It can be clearly observed from the Table 2a that RMSE for wheat NDVI using ARIMA model is minimum. Table 2b show RMSE error and MSE error for ARIMA, LSTM, and Prophet model using wheat BNDVI indices values. BNDVI indices for wheat crop show RMSE errors of 0.03, 0.0548 and 0.0748 for ARIMA, LSTM, and Prophet model respectively. It can be clearly observed from the Table 2b that RMSE for wheat BNDVI using ARIMA model is minimum. Table 2c show RMSE error and MSE error for ARIMA, LSTM, and Prophet model using wheat GNDVI indices values. GNDVI indices for wheat crop show RMSE errors of 0.02, 0.0509 and 0.0556 for ARIMA, LSTM, and Prophet model respectively. It can be clearly observed from the Table 2c that RMSE for wheat GNDVI using ARIMA model is minimum. Therefore, based on RMSE values,

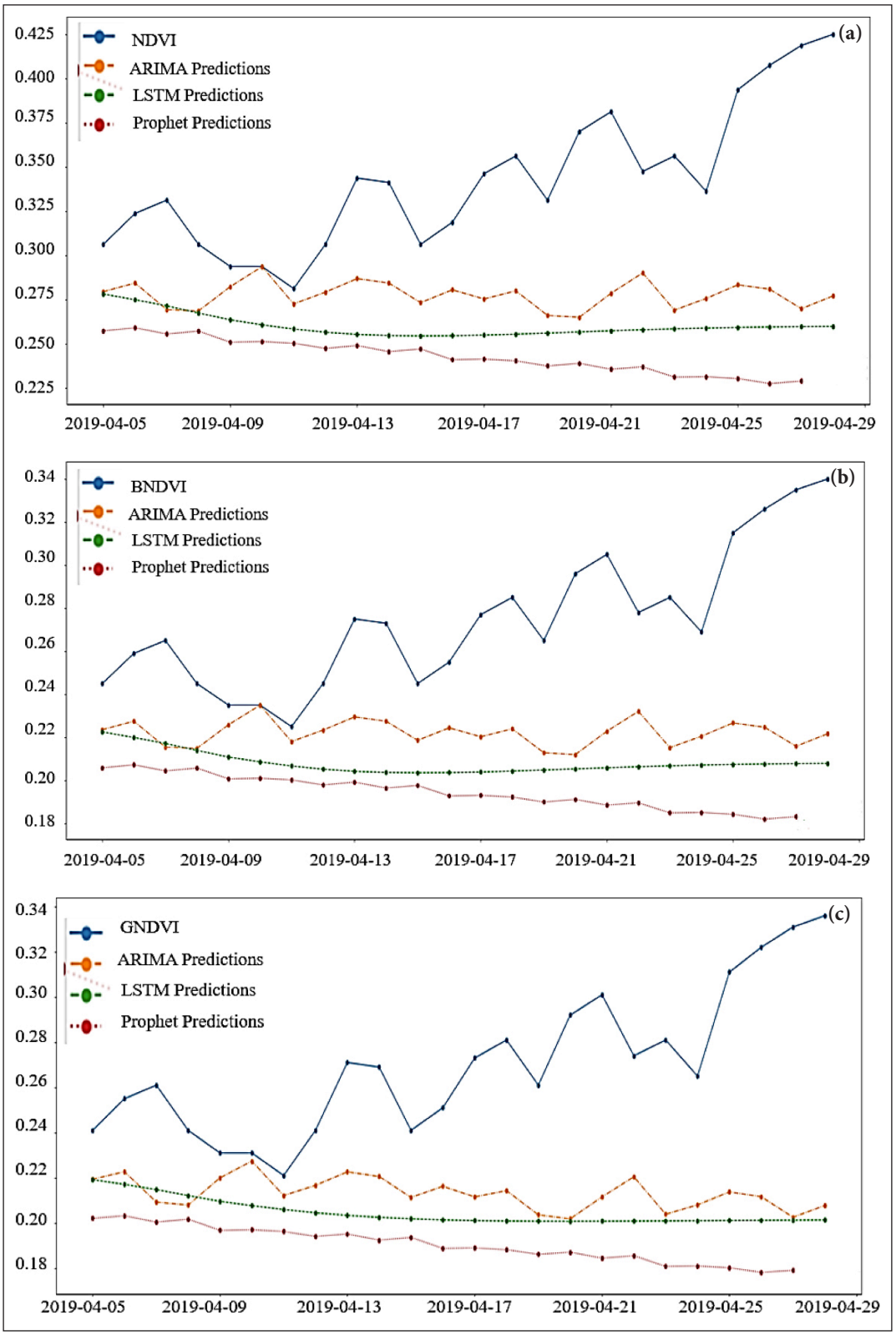


**Figure 5**. **(a)** NDVI indices predicted graph for ARIMA, LSTM and Prophet model. **(b)** BNDVI indices predicted graph for ARIMA, LSTM and Prophet model. **(c)** GNDVI indices predicted graph for ARIMA, LSTM and Prophet model.

ARIMA model may be selected to classify wheat crop using NDVI, BNDVI, GNDVI indices. For wheat crop, if we compare the RMSE values of NDVI, BNDVI and GNDVI. GNDVI indices shows minimum RMSE 0.02 using ARIMA model. NDVI indices shows minimum RMSE 0.0367 using LSTM model. GNDVI indices shows minimum RMSE 0.0556 using Prophet model. On the basis of these results, it may be analysed that to predict wheat crop, GNDVI indices are better for ARIMA and Prophet model and NDVI indices are better for LSTM model.

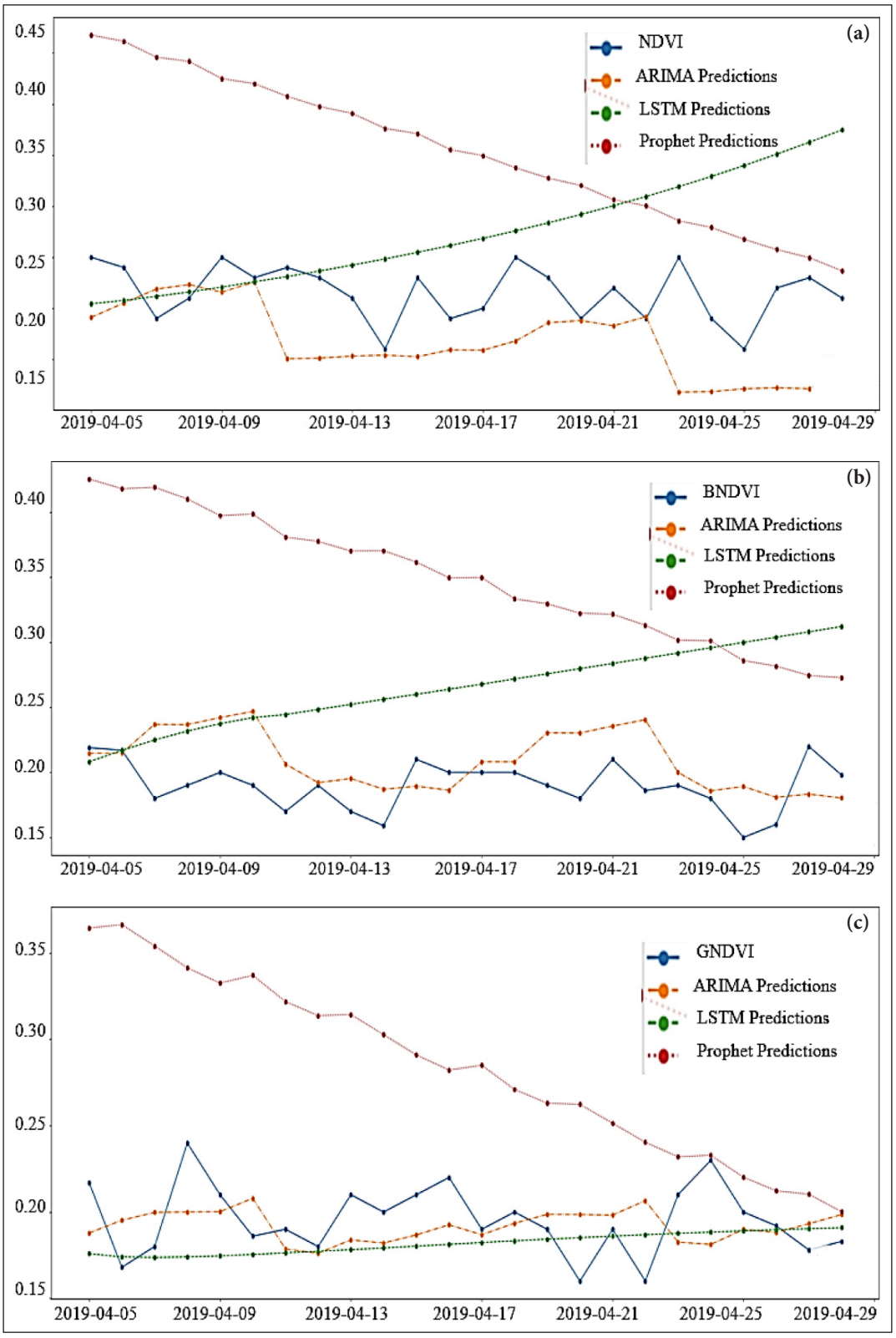


**Figure 6**. **(a)** NDVI indices predicted graph for ARIMA, LSTM and Prophet model. **(b)** BNDVI indices predicted graph for ARIMA, LSTM and Prophet model. **(c)** GNDVI indices predicted graph for ARIMA, LSTM and Prophet model.

***Sugarcane Crop***

Figure 5a, 5b and 5c showed NDVI, BNDVI, and GNDVI indices predicted graph for ARIMA, LSTM, and Prophet model for sugarcane crop. Table 3a show RMSE error and MSE error for ARIMA, LSTM, and Prophet model using sugarcane NDVI indices values. NDVI indices for sugarcane crop show RMSE errors of 0.0538, 0.0806 and 0.0883 for ARIMA, LSTM, and Prophet model respectively. It can be analysed from the Table 3a that RMSE for sugarcane NDVI using ARIMA model is minimum. Table 3b

show RMSE error and MSE error for ARIMA, LSTM, and Prophet model using sugarcane BNDVI indices values. BNDVI indices for sugarcane crop show RMSE errors of 0.0616, 0.0547 and 0.0889 for ARIMA, LSTM, and Prophet model respectively. It can be analysed from the Table 3b that RMSE for sugarcane BNDVI using LSTM model is minimum. Table 3c shows RMSE error for ARIMA, LSTM, and Prophet model using sugarcane GNDVI indices values. GNDVI indices for sugarcane crop show RMSE errors of 0.0670, 0.0741 and 0.0883 for ARIMA, LSTM, and Prophet model respectively. It can be analysed from the Table 3c that RMSE for sugarcane GNDVI using ARIMA model is minimum. Therefore, based on RMSE values, ARIMA model may be selected to classify sugarcane crop using NDVI and GNDVI indices. LSTM model may be selected to classify sugarcane crop using BNDVI indices. For sugarcane crop, if we compare the RMSE values of NDVI, BNDVI and GNDVI. NDVI indices shows minimum RMSE 0.0538 using ARIMA Model. BNDVI indices shows minimum RMSE 0.0547 using LSTM model. GNDVI indices shows minimum RMSE 0.067 using ARIMA model. On the basis of these results, it may be analysed that to predict sugarcane crop, NDVI and GNDVI indices are better for ARIMA model and BNDVI indices are better for LSTM model.

**Mustard Crop**

Figure 6a, 6b and 6c showed NDVI, BNDVI, and GNDVI indices predicted graph for ARIMA, LSTM, and Prophet model for mustard crop. Table 4a show RMSE error and MSE error for ARIMA, LSTM, and Prophet model using mustard NDVI indices values. NDVI indices for mustard crop show RMSE errors of 0.0632, 0.0860 and 0.1533 for ARIMA, LSTM, and Prophet model respectively. It can be analysed from the Table 4a that RMSE for mustard NDVI using ARIMA model is minimum. Table 4b show RMSE error and MSE error for ARIMA, LSTM, and Prophet model using mustard BNDVI indices values. BNDVI indices for mustard crop show RMSE errors of 0.0331, 0.0842 and 0.1655 for ARIMA, LSTM, and Prophet model respectively. It can be analysed from the Table 4b that RMSE for mustard BNDVI using ARIMA model is minimum. Table 4c show RMSE error and MSE error for ARIMA, LSTM, and Prophet model using mustard GNDVI indices values. GNDVI indices for mustard crop show RMSE errors of 0.0244, 0.0264 and 0.1019 for ARIMA, LSTM, and Prophet model respectively. It can be analysed from the Table 4c that RMSE for mustard GNDVI using ARIMA model is minimum. Therefore, based on RMSE values, ARIMA model may be selected to classify mustard crop using NDVI, BNDVI and GNDVI indices. For mustard crop, if we compare the RMSE values of NDVI, BNDVI and GNDVI. GNDVI indices shows minimum RMSE 0.0244 using ARIMA Model. GNDVI indices shows minimum MSE 0.0264 using LSTM model. GNDVI indices shows minimum MSE 0.1019 using Prophet model. On the basis of these results, it may be analysed that to predict mustard crop, GNDVI indices are best for ARIMA, Prophet, and LSTM model.

**Table 4a.** NDVI indices RMSE and MSE Errors for ARIMA, LSTM and Prophet model

| | Mustard NDVI | | |
|---|---|---|---|
| S. No. | Models | RMSE errors | MSE errors |
| 0 | ARIMA | 0.0632 | 0.0040 |
| 1 | LSTM | 0.0860 | 0.0074 |
| 2 | Prophet | 0.1533 | 0.0235 |

**Table 4b.** BNDVI indices RMSE and MSE Errors for ARIMA, LSTM and Prophet model

| | Mustard BNDVI | | |
|---|---|---|---|
| S. No. | Models | RMSE errors | MSE errors |
| 0 | ARIMA | 0.0331 | 0.0011 |
| 1 | LSTM | 0.0842 | 0.0071 |
| 2 | Prophet | 0.1655 | 0.0274 |

**Table 4c.** GNDVI indices RMSE and MSE Errors for ARIMA, LSTM and Prophet model

| | Mustard GNDVI | | |
|---|---|---|---|
| S. No. | Models | RMSE errors | MSE errors |
| 0 | ARIMA | 0.0244 | 0.0006 |
| 1 | LSTM | 0.0264 | 0.0007 |
| 2 | Prophet | 0.1019 | 0.0104 |

## CONCLUSION

In this Study ARIMA, LSTM and Prophet models are used to train the time series indices values (NDVI, BNDVI and GNDVI) of wheat, mustard and sugarcane crops of the study area. These models are used to analyse MSE and RMSE values by considering various parameters. For wheat crop, on the basis of individual vegetation indices, ARIMA model show least RMSE error of 0.0345 for NDVI indices, least RMSE error of 0.03 for BNDVI indices, and least RMSE error of 0.02 for GNDVI indices. So ARIMA model may be selected to classify wheat crop using NDVI, BNDVI, GNDVI indices. To predict wheat crop on the basis of model, GNDVI indices show least RMSE error of 0.02 for ARIMA model and least RMSE error of 0.0556 for Prophet model. NDVI indices show least RMSE error of 0.0367 for LSTM model. So GNDVI indices are better for ARIMA and Prophet model and NDVI indices are better for LSTM model. For sugarcane crop, on the basis of individual vegetation indices, ARIMA model show least RMSE error of 0.0538 for NDVI indices, LSTM model show least RMSE error of 0.0547 for BNDVI indices, and least RMSE error of 0.0741 for GNDVI indices. So ARIMA model may be selected to classify sugarcane crop using NDVI, LSTM model may be selected using BNDVI and GNDVI indices. To predict sugarcane crop on the basis of model, NDVI indices show least RMSE error of 0.0538 for ARIMA model, NDVI and GNDVI shows least RMSE error of 0.0883 for Proph-

et model. BNDVI indices show least RMSE error of 0.0547 for LSTM model. So NDVI indices are better for ARIMA model, NDVI and GNDVI indices are better for Prophet model and BNDVI indices are better for LSTM model. For mustard crop, on the basis of individual vegetation indices, ARIMA model show least RMSE error of 0.0632 for NDVI indices and least RMSE error of 0.0331 for BNDVI indices. LSTM model show least RMSE error of 0.0264 for GNDVI indices. So ARIMA model may be selected to classify mustard crop using NDVI, BNDVI indices and LSTM model may be selected using GNDVI indices. To predict mustard crop on the basis of model, GNDVI indices show least RMSE error of 0.0244 for ARIMA model, least RMSE error of 0.0264 for LSTM model, and least RMSE error of 0.1019 for Prophet model. So GNDVI indices are better for ARIMA, Prophet, and LSTM model. In order to analyse the crops of those localities that have similar environmental circumstances to the trained locale, the optimal model and vegetation indices may be chosen based on this training.

## DATA AVAILABILITY STATEMENT

The author confirm that the data that supports the findings of this study are available within the article. Raw data that support the finding of this study are available from the corresponding author, upon reasonable request.

## CONFLICT OF INTEREST

The author declared no potential conflicts of interest with respect to the research, authorship, and/or publication of this article.

## USE OF AI FOR WRITING ASSISTANCE

Not declared.

## ETHICS

There are no ethical issues with the publication of this manuscript.

## REFERENCES


[1] V. Avashia, S. Parihar, and A. Garg, "Evaluation of classification techniques for land use change mapping of Indian Cities," Journal of the Indian Society of Remote Sensing, Vol. 48(6), pp. 877–908, 2020. [CrossRef]

[2] P. Patil, V. Panpatil, and S. Kokate, "Crop prediction system using machine learning algorithms," International Research Journal of Engineering and Technology, Vol. 7(2), pp. 748–753, 2020.

[3] B. E. Bunker, "Classification of satellite time series-derived land surface phenology focused on the northern fertile crescent," [Dissertation thesis], University of Arkansas, 2013.

[4] X. X. Zhou, Y.-Y. Li, Y.-K. Luo, Y.-W. Sun, Y.-J. Su, C.-W. Tan, and Y.-J. Liu, "Research on remote sensing classification of fruit trees based on Sentinel-2 multi-temporal imageries," Scientific Reports, Vol. 12(1), 2022. [CrossRef]

[5] L. Wang, Q. Dong, L. Yang, J. Gao, and J. Liu, "Crop classification based on a novel feature filtering and enhancement method," Remote Sensing (Basel), Vol. 11(4), 2019. [CrossRef]

[6] E. Omia et al, H. Bae, E. Park, M. S. Kim, I. Baek, I. Kabenge, and B.-K. Cho, "Remote sensing in field crop Monitoring: A comprehensive review of sensor systems, data analyses and recent advances," Remote Sensing (Basel), Vol. 15(2), Article 354, 2023. [CrossRef]

[7] R. Filgueiras, E. C. Mantovani, D. Althoff, E. I. Fernandes Filho, and F. F. da Cunha, "Crop NDVI monitoring based on sentinel 1," Remote Sensing (Basel), Vol. 11(12), 2019. [CrossRef]

[8] A. Orynbaikyzy, U. Gessner, B. Mack, and C. Conrad, "Crop type classification using fusion of sentinel-1 and sentinel-2 data: Assessing the impact of feature selection, optical data availability, and parcel sizes on the accuracies," Remote Sensing (Basel), Vol. 12(17), 2020. [CrossRef]

[9] P. Hao, L. Wang, and Z. Niu, "Comparison of hybrid classifiers for crop classification using normalized difference vegetation index time series: A case study for major crops in North Xinjiang, China," PLoS One, Vol. 10(9), Article 0137748, 2015. [CrossRef]

[10] Q. Li, J. Tian, and Q. Tian, "Deep Learning application for crop classification via multi-temporal remote sensing images," Agriculture (Switzerland), Vol. 13(4), Article 906, 2023. [CrossRef]

[11] J. Dyson, A. Mancini, E. Frontoni, and P. Zingaretti, "Deep learning for soil and crop segmentation from remotely sensed data," Remote Sensing (Basel), Vol. 11(16), Article 1859, 2019. [CrossRef]

[12] N. Yang, D. Liu, Q. Feng, Q. Xiong, L. Zhang, T. Ren, … and J. Huang, "Large-scale crop mapping based on machine learning and parallel computation with grids," Remote Sensing (Basel), Vol. 11(12), Article 1500, 2019. [CrossRef]

[13] G. A. Abubakar, K. Wang, A. R. Shahtahamssebi, X. Xue, M. Belete, A. J. Abdallah Gudo, … and M. Gan, "Mapping maize fields by using multi-temporal sentinel-1a and sentinel-2a images in Makarfi, Northern Nigeria, Africa," Sustainability (Switzerland), Vol. 12(6), Article 2539, 2020. [CrossRef]

[14] X. Guan, C. Huang, G. Liu, X. Meng, and Q. Liu, "Mapping rice cropping systems in Vietnam using an NDVI-based time-series similarity measurement based on DTW distance," Remote Sens (Basel), Vol. 8(1), Article 19, 2016. [CrossRef]

[15] J. Senthilnath, S. Kulkarni, J. A. Benediktsson, and X. S. Yang, "A novel approach for multispectral satellite image classification based on the bat algorithm," IEEE Geoscience and Remote Sensing Letters, Vol. 13(4), pp. 599–603, 2016. [CrossRef]

[16] X. Zhang, Y. Sun, K. Shang, L. Zhang, and S. Wang, "Crop classification based on feature band set construction and object-oriented approach using hyperspectral images," IEEE Journal of Selected Topics in Applied Earth Observations and Remote Sensing, Vol. 9(9), pp. 4117–4128, 2016. [CrossRef]

[17] S. Siachalou, G. Mallinis, and M. Tsakiri-Strati, "Analysis of time-series spectral index data to enhance crop identification over a mediterranean rural landscape," IEEE Geoscience and Remote Sensing Letters, Vol. 14(9), pp. 1508–1512, 2017. [CrossRef]

[18] M. Pasternak, and K. Pawluszek-Filipiak, "The evaluation of spectral vegetation indexes and redundancy reduction on the accuracy of crop type detection," Applied Sciences (Switzerland), Vol. 12(10), Aricle 5067, 2022. [CrossRef]

[19] Y. Palchowdhuri, R. Valcarce-Diñeiro, P. King, and M. Sanabria-Soto, "Classification of multi-temporal spectral indices for crop type mapping: A case study in Coalville, UK," Journal of Agricultural Science, Vol. 156(1), pp. 24–36, 2018. [CrossRef]

[20] R. Sonobe, Y. Yamaya, H. Tani, X. Wang, N. Kobayashi, and K. Mochizuki, "Crop classification from Sentinel-2-derived vegetation indices using ensemble learning," Journal of Applied Remote Sensing, Vol. 12(02), pp. 1, 2018. [CrossRef]

[21] N. Kobayashi, H. Tani, X. Wang, and R. Sonobe, "Crop classification using spectral indices derived from sentinel-2a imagery," Journal of Information and Telecommunication, Vol. 4(1), pp. 67–90, 2020. [CrossRef]

[22] H. Tian, N. Huang, Z. Niu, Y. Qin, J. Pei, and J. Wang, "Mapping winter crops in China with multi-source satellite imagery and phenology-based algorithm," Remote Sensing (Basel), Vol. 11(7), 2019. [CrossRef]

[23] E. Akbari, A. D. Boloorani, N. N. Samany, S. Hamzeh, S. Soufizadeh, and S. Pignatti, "Crop mapping using random forest and particle swarm optimization based on multi-temporal sentinel-2," Remote Sensing (Basel), Vol. 12(9), 2020. [CrossRef]

[24] K. Goldberg, I. Herrmann, U. Hochberg, and O. Rozenstein, "Generating up-to-date crop maps optimized for sentinel-2 imagery in Israel," Remote Sensing (Basel), Vol. 13(17), 2021. [CrossRef]

[25] Y. Kang, X. Hu, Q. Meng, Y. Zou, L. Zhang, M. Liu, and M. Zhao, "Land cover and crop classification based on red edge indices features of gf-6 wfv time series data," Remote Sensing (Basel), Vol. 13(22), Article 4522, 2021. [CrossRef]

[26] Y. Hu, H. Zeng, F. Tian, M. Zhang, B. Wu, S. Gilliams, … and H. Yang, et al., "An interannual transfer learning approach for crop classification in the Hetao Irrigation District, China," Remote Sensing (Basel), Vol. 14(5), Article 1208, 2022. [CrossRef]

[27] K. Ravali, and M. Teng-Sheng, Machine Learning in Indian Crop Classification of Temporal Multi-Spectral Satellite Image, 14th IMCOM 2020. Taichung, Taiwan, 2020.

[28] K. Aleem, P. Leonardo, and C. Marcello, "Land cover and crop classification using multitemporal sentinel-2 images based on crops phenological Cycle," IEEE Workshop EESMS. Salerno, Italy, 2018.

[29] X. Chen, Y. Zhan, Y. Liu, X. Gu, T. Yu, … and Y. Zhang, "Improving the classification accuracy of annual crops using time series of temperature and vegetation indices," Remote Sensing (Basel), Vol. 12(19), Article 3202, 2020. [CrossRef]

[30] F. Carreño-Conde, A. E. Sipols, C. Simón, and D. Mostaza-Colado, "A forecast model applied to monitor crops dynamics using vegetation indices (Ndvi)," Applied Sciences (Switzerland), Vol. 11(4), pp. 1–25, 2021. [CrossRef]

[31] R. Sonobe, Y. Yamaya, H. Tani, X. Wang, N. Kobayashi, and K. ichiro Mochizuki, "Assessing the suitability of data from Sentinel-1A and 2A for crop classification," GIsci Remote Sensing, Vol. 54(6), pp. 918–938, 2017. [CrossRef]

[32] R. Azar, P. Villa, D. Stroppiana, A. Crema, M. Boschetti, and P. A. Brivio, "Assessing in-season crop classification performance using satellite data: A test case in Northern Italy," European Journal of Remote Sensing, Vol. 49, pp. 361–380, 2016. [CrossRef]

[33] A. Bouguettaya, H. Zarzour, A. Kechida, and A. M. Taberkit, "Deep learning techniques to classify agricultural crops through UAV imagery: a review," Neural Computing and Applications, Vol. 34(12), pp. 9511–9536, 2022. [CrossRef]

[34] N. Kussul, M. Lavreniuk, S. Skakun, and A. Shelestov, "Deep learning classification of land cover and crop types using remote sensing data," IEEE Geoscience and Remote Sensing Letters, Vol. 14(5), pp. 778–782, 2017. [CrossRef]

[35] N. Kussul, S. Skakun, A. Shelestov, M. Lavreniuk, B. Yailymov, and O. Kussul, "Regional scale crop mapping using multi-temporal satellite imagery," in International Archives of the Photogrammetry, Remote Sensing and Spatial Information Sciences - ISPRS Archives, International Society for Photogrammetry and Remote Sensing, 2015, pp. 45–52, 2015. [CrossRef]

[36] N. Kussul, G. Lemoine, F. J. Gallego, S. V. Skakun, M. Lavreniuk, and A. Y. Shelestov, "Parcel-Based Crop Classification in Ukraine Using Landsat-8 Data and Sentinel-1A Data," IEEE Journal of Selected Topics in Applied Earth Observations and Remote Sensing, Vol. 9(6), pp. 2500–2508, 2016. [CrossRef]

[37] L. Pan, H. Xia, X. Zhao, Y. Guo, and Y. Qin, "Mapping winter crops using a phenology algorithm, time-series sentinel-2 and landsat-7/8 images, and google earth engine," Remote Sens (Basel), Vol. 13(13), Article 2510, 2021. [CrossRef]